The genomes of nematode-trapping fungi provide insights into the origin and diversification of fungal carnivorism

Yani Fan [a,c,1], Minghao Du [b,1], Weiwei Zhang [a,c,1], Wei Deng [d,1], Ence Yang [b], Shunxian Wang [d], Luwen Yan [d], Liao Zhang [d], Seogchan Kang [e], Jacob L Steenwyk [f], Zhiqiang An [g], Xingzhong Liu [a,d,*] , Meichun Xiang [a,c,*]

[a] State Key Laboratory of Microbial Diversity and Innovative Utilization, Institute of Microbiology, Chinese Academy of Sciences, Beijing 100101, China
[b] Department of Microbiology, School of Basic Medical Sciences, Peking University Health Science Center, Beijing 100191, China
[c] University of Chinese Academy of Sciences, Beijing 100049, China
[d] State Key Laboratory of Medicinal Chemical Biology, Key Laboratory of Molecular Microbiology and Technology of the Ministry of Education, Department of Microbiology, College of Life Science, Nankai University, Tianjin 300071, China
[e] Department of Plant Pathology & Environmental Microbiology, Pennsylvania State University, PA 16802, USA
[f] Howards Hughes Medical Institute and Department of Molecular and Cell Biology, University of California, Berkeley, CA 94720, USA
[g] Texas Therapeutics Institute, The Brown Foundation Institute of Molecular Medicine, University of Texas Health Science Center, Houston, TX 77030, USA

ABSTRACT

Nematode-trapping fungi (NTF), most of which belong to a monophyletic lineage in Ascomycota, cannibalize nematodes and other microscopic animals, raising questions regarding the types and mechanisms of genomic changes that enabled carnivorism and adaptation to the carbon-rich and nitrogen-poor environment created by the Permian-Triassic extinction event. To address these questions, we conducted comparative genomic analyses of 21 NTF and 21 non-NTF. Carnivorism-associated changes include expanded genes for nematode capture, infection, and consumption (e.g., adhesive proteins, CAP superfamily, eukaryotic aspartyl proteases, and serine-type peptidases). Although the link between secondary metabolite (SM) production and carnivorism remains unclear, we found that the number of SM gene clusters in NTF was significantly lower than that in non-NTF. Significantly expanded cellulose degradation gene families (GH5, GH7, AA9, and CBM1) and contracted genes for carbon–nitrogen hydrolases (enzymes that degrade organic nitrogen to ammonia) are likely associated with adaptation to carbon-rich and nitrogen-poor environments. Through horizontal gene transfer events from bacteria, NTF acquired the *Mur* gene cluster (participating in synthesizing peptidoglycan of the bacterial cell wall) and *Hyl* (a virulence factor in animals). Disruption of *MurE* reduced NTF's ability to attract nematodes, supporting its role in carnivorism. This study provides new insights into how NTF evolved and diversified, presumably after the Permian-Triassic mass extinction event.

1. Introduction

Fungi employ diverse strategies to acquire nutrients for growth and reproduction. Carnivorous nematode-trapping fungi (NTF) have evolved sophisticated trapping devices to capture and consume nematodes and other microscopic animals, such as amoebas, rotifers, and springtails (Pramer, 1964). Although carnivorous fungi have been found in multiple phyla, more than 90 % of the known NTF belong to the class Orbiliomycetes, a monophyletic lineage in Ascomycota (Yang et al., 2007).

Ascomycota NTF develop adhesive traps and constricting rings to capture and consume nematodes, the most abundant soil animals (Nordbring-Hertz and Stålhammar-Carlemalm, 1978; van den Hoogen et al., 2019). The rarity of carnivorism among fungi has raised great interest in unraveling the origin and evolution of carnivorous traits.

The evolution of carnivorous Orbiliomycetes has been studied using multilocus phylogenetic analyses (Li et al., 2005; Yang et al., 2007, 2012). Previous studies suggested that the origin of NTF might be related to the Permian-Triassic mass extinction event (Yang et al., 2012).

The collapse of terrestrial ecosystems during this event markedly increased the amount of dead plant material, creating carbon-rich environments (Visscher et al., 1996). Concurrently, marine nitrogen cycling shifted to an ammonium-dominated state owing to nitrate depletion and intensified nitrogen fixation under prolonged oceanic anoxia (Romano et al., 2013; Sun et al., 2019), resulting in nitrogen-poor conditions. These parallel terrestrial and marine perturbations, driven by Siberian Traps volcanism (Blackburn et al., 2013), caused extreme global warming (Benton and Twichett, 2003) and carbon cycle destabilization (Shen et al., 2011). These events collectively created a carbon-rich and nitrogen-poor environment. Barron (2003) hypothesized that NTF evolved the ability to capture nematodes to supplement nitrogen. Several NTF traits support this hypothesis. First, trap morphogenesis is induced only when free-living nematodes are present and usually requires physical contact between the hyphae and nematodes (Tunlid et al., 1992; Vidal-Diez de Ulzurrun and Hsueh, 2018). Second, NTF actively attract nematodes to their mycelia and hold them during trap formation (Lopez-Llorca et al., 2007; Vidal-Diez de Ulzurrun and Hsueh, 2018). In addition, NTF's high lignolytic and cellulolytic activities, which are advantageous for living in carbon-rich environments, have been well documented (Barron, 2003, 1992).

Comparative and evolutionary genomics has shed light on niche adaptation and the evolution of genotype-phenotype maps across diverse lineages (Bajic and Sanchez, 2020; Malar et al., 2021; Murat et al., 2018; Smith et al., 2020; Steenwyk and Rokas, 2017). For example, a study of Saccharomycotina yeasts revealed that adaptation to nitrogen-poor environments involves gene family contractions (e.g., nitrogen hydrolases) and expansions (e.g., *MAL/IMA* genes), resulting in metabolic rewiring (Opulente et al., 2024). Similarly, genomic analyses of lignin-degrading mushroom-forming fungi demonstrated that lineage-specific expansions of oxidoreductases (Class II peroxidases MnP/LiP, laccases) and CAZymes (e.g., GH6 and GH7) underpin complex substrate degradation, which was validated by transcriptomics and microscopy (Floudas et al., 2012). Accordingly, comparative genome analyses between NTF and non-NTF hold promise to uncover candidate genomic changes underlying the evolution of nematode-trapping capabilities, such as protease expansion for prey digestion.

Genome sequences of the Orbiliomycetes, an early branch of Ascomycota, became available only in 2011. Since the sequencing of *Arthrobotrys oligospora* (Yang et al., 2011), eight species (seven NTF and one non-NTF) of the Orbiliomycetes have been sequenced. Here, we conducted comparative phylogenomic analyses of 21 NTF (16 of which were first sequenced and assembled in this study) and 21 non-NTF Ascomycota species to elucidate the nature of their genomic adaptations to fungal carnivores. Our investigation identified potential genomic changes associated with carnivorism, such as horizontally transferred bacterial genes (e.g., *MurE* involved in nematode attraction) and genes associated with adaptations to carbon-rich/nitrogen-poor environments (e.g., contracted nitrogen hydrolases). Transcriptome analysis of three NTF (*Drechslerella dactyloides*, *Dactylellina haptotyla*, and *Arthrobotrys oligospora*) in the absence and presence of the nematode *Caenorhabditis elegans* (Fan et al., 2021; Yang et al., 2022) revealed upregulation of candidate genes associated with carnivory, such as adhesive protein-coding genes, in the presence of nematodes. Furthermore, targeted disruption of *MurE* confirmed its importance in carnivorism. Collectively, these analyses revealed multiple genomic changes that likely contributed to the evolutionary trajectory of NTF.

2. Materials and methods

2.1. Strains, media, and culturing conditions

The NTF sequenced (Supplementary Table 1) were cultured on potato dextrose agar (PDA) and corn meal agar (CMA). Mycelia used for genomic DNA extraction were prepared by inoculating approximately 10^5 spores or ten 5-mm diameter plugs from a freshly grown culture on PDA into 100 mL potato dextrose broth (PDB). After shaking the cultures at 120 rpm and 28 °C for 10 days, the resulting mycelia were collected using a glass cotton filter and washed three times with distilled water.

2.2. Whole-genome sequencing

Genomic DNA was extracted using a CTAB/SDS/Proteinase K method (Möller et al., 1992). Four genomic DNA libraries with insert sizes of 400 bp, 500 bp, 3 kb, and 5–8 kb were prepared. The library with 400 bp inserts was sequenced using Illumina PE250. The remaining libraries were sequenced using the Illumina PE150. The resulting sequence reads were processed using Trimmomatic v0.38 to remove adapters and low-quality reads (Bolger et al., 2014). Processed reads were assembled *de novo* using Allpaths-LG v52488 (Gnerre et al., 2011) with SPAdes (k = 33, 55, 66, 99; −-cov-cutoff auto) to optimize assembly based on read depth. To improve completeness, draft assembled genomes were scaffolded using data from mate-pair libraries (3 Kb and 5–8 Kb) via two rounds of SSPACE-standard v3.0 (minimum links = 5) (Boetzer et al., 2011). The output was used for the analyses described below. The completeness of individual genome assemblies and gene prediction was evaluated using BUSCO v4.0.2, based on the Ascomycota ortholog database containing 1,706 orthologs.

2.3. Gene prediction and functional annotation

Regions of repetitive sequence elements in the assembly were masked using RepeatMasker v4.0.7 based on a species-specific repeat library generated using RepeatModeler v4.0.7. For structural annotation, the quality of protein sequence predictions was assessed using BUSCO analysis. The BRAKER pipeline (Hoff et al., 2016) was used to test protein homology. For functional annotation, the final gene set for each species was analyzed using Pfam, PRINTS, PANTHER, SUPERFAMILY, SMART, and Gene 3D in InterProScan v5.39-77.0 (Jones et al., 2014).

The carbohydrate-active enzymes (CAZymes) were predicted by aligning all protein-coding genes in each species against the dbCAN2 database (Zhang et al., 2018) using DIAMOND v0.9.24.125, HMMER v3.0, and Hotpep. Those supported by more than two aligners were considered as CAZymes. The Secondary Metabolite Unknown Regions Finder (SMURF) was used to predict SM gene clusters (Khaldi et al., 2010). Secreted proteins were identified using multiple processes. SignalP v5.1 (Almagro Armenteros et al., 2019) was initially used to predict candidates. Subsequently, putative membrane proteins were filtered out using TMHMM v2.0 (Krogh et al., 2001). Likely mitochondrial or endoplasmic reticulum proteins were removed using WoLF PSORT, TargetP v2.0, and Deeploc v2.0 (Armenteros et al., 2019; Horton et al., 2007; Thumuluri et al., 2022).

2.4. Phylogenomic data matrix construction and analysis

Concatenation is a popular method for inferring organismal histories (Steenwyk et al., 2023) and has been successfully used to infer evolutionary relationships in fungi (Li et al., 2021). Orthologous relationships among the genes in 21 NTF and 21 non-NTF were determined using OrthoFinder v2.2.6, with default settings (Emms and Kelly, 2019). Single-copy genes present in all species were used for phylogenetic analysis. For each group of single-copy orthologous genes, their predicted protein sequences were aligned using MAFFT v7.453 (Katoh and Standley, 2013). Aligned sequences were trimmed using the "gappyout" model in trimAl v1.5 (Capella-Gutiérrez et al., 2009), which has been demonstrated to be an efficacious approach for trimming (Steenwyk et al., 2020a; Tan et al., 2015), and concatenated. A maximum likelihood tree was generated using RAxML v8.2.12 (Stamatakis, 2014) under the Q.insect + F + I + R10 model, which was automatically selected, with a discrete gamma distribution of rates across sites. 1,000 bootstrap resamplings were performed to evaluate bipartition support.

2.5. Divergence time estimation

To precisely infer the origin time of NTF, we incorporated two well-characterized outgroup calibration species with established divergence times, *Saccharomyces cerevisiae* (GCF_000146045.2) and *Ustilago maydis* (GCF_000328475.2), into a dataset comprising 21 NTF species and 21 non-NTF Ascomycota taxa. Orthologous gene analysis was performed using OrthoFinder v2.2.6, with default thresholds of 50 % site coverage and an e-value of $\leq$ 1e−5 (Emms and Kelly, 2019), identifying 364 single-copy orthologous gene families.

Multiple sequence alignment was conducted using MAFFT v7.453 (Katoh and Standley, 2013), followed by conservative site filtering using trimAl v1.5 (Capella-Gutiérrez et al., 2009). Quality-controlled alignments were concatenated into a supermatrix (total length: 157,374 bp). Phylogenetic reconstruction was performed in IQ-TREE v2.2.2.7 (parameters: −m TESTNEW −B 1000 −alrt 1000 −T AUTO), with the ModelFinder module selecting Q.yeast + F + I + G4 as the optimal substitution model (Minh et al., 2020; Kalyaanamoorthy et al., 2017).

Divergence time estimation was implemented using two complementary approaches: 1. RelTime-ML (MEGA 11) (Tamura et al., 2021): Calibrated using Saccharomycotina origin time (438.4 MYA, 95 % CI: 304–590 MYA) (Shen et al., 2020). 2. r8s (Sanderson, 2003): Employed cross-validation (parameters: cvStart = 0, cvInc = 0.5, cvNum = 8) with a hard calibration point for the Basidiomycota-Ascomycota divergence (642 MYA, CI: 583.2–749.0 MYA) (Shen et al., 2020) under a penalised likelihood (PL) framework with TN optimisation. Both methods utilized identically rooted phylogenetic trees and sequence data. Reliability was validated by comparing node age confidence interval overlaps with a particular focus on NTF clade origins. Final chronograms were visualized using FigTree v1.4.4 (https://tree.bio.ed.ac.uk/software/figtree/).

2.6. Analysis of Pfam domains

To characterize the patterns of functional diversification in functional domains across the NTF genomes, the copy numbers of each Pfam domain in 21 NTF and 21 non-NTF were subjected to principal component analysis (PCA) using the "prcomp" function in the stat package of R v4.2.3 with default settings (R Core Team, 2023). We ranked the contribution to the first principal component (PC1) in descending order and selected the top 10 % to display via a heatmap using the Pheatmap v1.0.12 package of R (Kolde, 2019). The number of Pfam domains for each species was normalized using zero-mean normalization, and the corresponding profiles were shown in the heatmap.

2.7. Statistical analysis

Enrichment analysis of Pfam domains in NTF-specific genes was performed using the Mann-Whitney *U* test. The *p*-values were corrected using the Bonferroni method. Comparison of the number of CAZymes involved in cellulose degradation with or without carbohydrate-binding module (CBM) between NTF and non-NTF was carried out using Mann-Whitney *U* test utilizing "wilcox.test" function in the stat package of R. The results were visualized using the ggplot2 package v3.3.2 of R (Wickham, 2017).

2.8. Transcriptome analysis

Published transcriptome data of *D. dactyloides* (Accession: PRJNA723922), which forms constricting rings, and *A. oligospora* (Accession: PRJNA791406), which forms adhesive nets, were downloaded from GenBank (Fan et al., 2021; Yang et al., 2022), and transcriptome data of *Da. haptotyla*, which forms adhesive knobs, were generated by us (unpublished but corresponding transcriptomic datasets are offered in supplementary tables 15–19). The sampling method is as follows: approximately 10^5 conidia were cultured on water agar plates overlaid with sterilized cellophane for 3 days at 25°C. Mycelia were harvested before exposure to 1,000 *Caenorhabditis elegans* and 24 hr after exposure. Normalized read counts were used to estimate gene expression levels using DESeq2's default size factor normalization. Genes with low expression levels (read counts < 5) were removed. The expression levels of the genes predicted to be involved in niche adaptation based on our comparative genome analysis were compared in the presence (24 hr) and absence (0 hr) of *C. elegans*. Genes with padj < 0.05 and |log2 Foldchange| >1 were considered differentially expressed.

2.9. MurE disruption and nematode attraction assay

The disruption of *DdaMurE* in *D. dactyloides* strain 29 (CGMCC3.20198) was conducted using a modified *Agrobacterium tumefaciens*-mediated transformation protocol (Fan et al., 2021). The same length of homologous arms, transformation conditions, transformant screening strategy, and qPCR validation were used. Nematode attraction assays were performed using a zoned plate method (Detailed information refer to Fig. S1 and Fig. S2). *D. dactyloides* strain 29 (WT) and three *ΔDdaMurE* mutants of strain 29 were cultured on PDA at 25°C for 14 days, with 6-mm mycelial plugs collected from colony margins. The mycelial plug and sterile PDA plug control were placed in designated rings on pre-divided water agar plates (90 mm), with five replicates for each sample. Two hundred *C. elegans* were added to the central location (a circle with a radius of 0.5 cm), and after incubating the inoculated plates for 6 hr at 25°C in the dark, the attractive indexes were calculated. We used the attractiveness index system described by Le Saux and Quénéhervé (2002). The system quantifies the degree of attraction or repulsion using numbers ranging from + 2 (attraction) to −2 (repulsion). The resulting data were analyzed using R, and significant differences were determined by a *p*-value < 0.01 using Student's *t*-test.

3. Results

3.1. Characteristics of the NTF genomes

The NTF genomes analyzed (16 *de novo* sequenced and 5 downloaded from GenBank) included 4 *Drechslerella* spp. forming mechanical constricting rings, 9 *Arthrobotrys* spp. forming 3-dimensional (3-D) adhesive nets, 8 *Dactylellina* spp. forming 2-D traps with the exception of *Da. cionopaga* (forming adhesive columns), and 7 other species forming adhesive knobs (Supplementary Table 1). Genome sizes ranged from 30.2 to 54.2 Mb (median 39.0 Mb), with the number of predicted protein-coding genes varying from 7,955 to 13,112 (Table 1) and 60.9–70.0 % of the genes being annotated to encode proteins with Pfam domain(s). Although the N50 values of the *Da. entomopaga* (579 Kb), *Da. haptotyla* (177 Kb) and *Da. drechsleri* (743 Kb) genomes were much lower than those of the other NTF genomes (1.2–6.2 Mb), examination of near-universally single-copy orthologs (or BUSCO genes) indicated high gene content completeness (93.7–96.1 %). RelTime-ML analyses estimated the divergence time between NTF and non-NTF at 250.03 MYA (95 % confidence interval: 156.81–398.65 MYA), while r8s gave a similar estimate of 252.70 MYA (Fig. S3). This timing aligns with the PT mass extinction (252 MYA) (Wu et al., 2024).

We compared the 21 NTF genomes with those of 21 non-NTF species (Ascomycota) representing diverse lifestyles, including saprophytic, mutualistic, phytopathogenic, endophytic, entomopathogenic, and nematode endoparasitic (Fig. 1A; Supplementary Table 2). We identified 22,679 orthologous groups (OGs) among the 458,922 protein-coding genes on the 42 genomes using OrthoFinder (Supplementary Table 3). We defined the OGs shared by all fungi as fungal-conserved, the OGs unique to each species as species-specific, and the OGs present in two or more NTF genomes but absent in non-NTF genomes as NTF-specific. All other OGs were classified as Other. Species-specific OGs account for 0–6.3 %, and 25.1–47.2 % of the OGs in each species are present in all 42

Table 1
Genome features of 21 nematode-trapping fungi.

Species[a]	Size (Mb)	N50 (Mb)	GC (%)	No. genes	Pfam (%)	BUSCO (%)
Arthrobotrys conoides	39.8	1.8	42.7	10,254	63.1	94.3
A. iridis	39.8	2.5	44.4	10,158	64.7	95.0
A. musiformis	40.8	2.0	44.3	10,510	63.0	95.1
A. oligospora	40.1	2.0	44.5	10,779	62.3	94.1
A. pseudoclavata	35.1	6.0	45.9	9,356	66.1	95.2
A. sinensis	40.6	2.3	45.6	11,240	62.1	95.5
A. sphaeroides	40.6	2.3	46.7	10,643	63.0	95.6
A. vermicola	40.7	1.6	45.6	10,501	63.0	95.7
A. flagrans	36.6	6.2	45	9927	68.2	93.4
Dactylellina cionopaga	47.4	2.1	43.8	12,524	61.5	93.8
Da. entomopaga	38.4	0.6	45	10,470	61.0	94.6
Da. drechsleri	54.2	0.7	38.4	11,044	63.1	93.8
Da. haptotyla	38.9	0.2	45.7	10,353	65.1	94.5
Da. leptospora	36.9	1.2	44.6	9,986	65.4	94.5
Da. parvicollis	38.3	1.7	46.0	10,329	64.7	94.7
Da. querci	34.4	3.1	46.0	9,718	65.5	93.8
Da. tibetensis	36.4	1.9	45.1	10,165	65.6	93.7
Drechslerella brochopaga	35.8	1.9	50.5	9,044	67.1	96.1
Dr. coelobrocha	36.4	2.9	46.9	9,495	66.3	95.3
Dr. dactyloides	37.7	1.3	50.3	8,978	67.2	96.1
Dr. stenobrocha	30.2	4.8	50.4	7,955	70.0	94.5

[a] The sources of the sequenced strains and their accession numbers are shown in Supplementary Table 1.

genomes (Fig. 1B; Supplementary Table 4). In total, 514 OGs are NTF-specific and present in all NTF, accounting for 5.4–6.8 % of the total genes in each species (Fig. 1B; Supplementary Table 5). However, 65.4 % of the NTF-specific OGs could not be annotated (orphan genes). Some OGs are unique to each NTF lineage and may be associated with unique trapping strategies: 52 OGs in 3-D adhesive net-forming species, 16 OGs in 2-D adhesive net-forming species, and 31 OGs in mechanical trap-forming species.

Functional enrichment analysis of the NTF-specific OGs containing Pfam domain(s) showed significant enrichment of multiple gene families related to nematode capture (CFEM domain and putative adhesin), infection, and digestion [cysteine-rich secretory protein family (CAP superfamily), eukaryotic aspartyl protease (ASP), and subtilase family]. In addition, cellulose-binding domains (fungal cellulose-binding domain and WSC domains), protein ubiquitination degradation-related domains (F-box domain and ubiquitin-conjugating enzyme), amino acid permeases, and Mur proteins (involved in synthesizing peptidoglycan, a main component of the bacterial cell wall) are significantly enriched in the NTF-specific OGs (Fig. 1C; Supplementary Table 7). A search of the Non-Redundant Protein Sequence Database using the 514 NTF-specific OGs and subsequent HGTector2 analysis revealed 89 putative horizontal gene transfer (HGT) events (Zhu et al., 2014). Four OGs containing different Mur protein domains and one OG with a "polysaccharide lyase family 8 domain" may participate in carnivorism. These domains exhibit significant sequence similarity to bacterial proteins but lack homologous fungal proteins (e = 1e-5, Supplementary Table 8), suggesting their horizontal gene transfer (HGT) from bacteria.

Principal component analysis (PCA) revealed significant differences in the conserved Pfam domains between NTF and non-NTF. NTF formed a discrete cluster separated from non-NTF according to PC1 (Fig. 2A). The Pfam domains that contributed the most (top 10 %, 451 Pfam domains) to PC1 included 153 expanded and 298 contracted domains (Fig. 2B; Supplementary Table 9). The expanded genes include (a) those encoding extracellular proteins such as "Egh16-like virulence factor" and "cysteine-rich secretory protein family", (b) proteases such as "Matrixin", protein ubiquitination degradation-related domains such as "F box", and (c) cellulose-binding modules such as "fungal cellulose-binding domain". In contrast, the genes for carbon–nitrogen

hydrolases and secondary metabolism, such as "cytochrome P450", "polyketide synthase dehydratase", and "acyl transferase domain", were contracted (Supplementary Table 9).

3.2. Genome changes likely associated with adaptation to carbon-rich and nitrogen-poor environments

The hypothesis that fungal carnivorism evolved in response to mass extinction was proposed (Barron, 2003) but has not been tested (Yang et al., 2012). Analysis of the gene families involved in carbohydrate metabolism (Supplementary Table 10) showed that the number of carbohydrate-active enzyme (CAZyme) genes ranged from 278 to 500 in NTF (mean of 409), which is significantly lower than that in plant-associated non-NTF (endophytic: mean of 786, $p = 0.0252$; phytopathogenic: mean of 591, $p = 0.0007$; mutualistic: mean of 570, $p = 0.0085$) but significantly higher than that in animal parasitic non-NTF, such as entomopathogenic (mean of 352, $p = 0.0027$) and nematode-endoparasitic fungi (mean of 269, $p = 0.0333$) (Fig. 3A). Moderate expansion of the genes encoding cellulose-degrading enzymes, including GH5, GH7, and AA9, in NTF likely enhanced their cellulose-degrading capability. Moreover, the NTF genomes encode a larger set of proteins carrying one or more carbohydrate-binding modules (CBM) compared to the non-NTF genomes (Fig. 3B). CBMs, particularly CBM1 (Chundawat et al., 2021), are essential for cellulases to bind to the cellulose surface, thereby enhancing the efficiency of cellulose-degrading enzymes (Espagne et al., 2008; Klosterman et al., 2011; Liu et al., 2014). The number of cellulose-degrading enzymes with CBM1 in NTF is much higher than that in non-NTF (Mann-Whitney U test) (Fig. 3C; Supplementary Table 11), a feature that likely enhanced NTF's ability to degrade cellulose.

Carnivorous fungi prey on nematodes to supplement their nitrogen intake (Barron, 2003; Lee et al., 2020; Yang et al., 2012). The gene family encoding carbon–nitrogen hydrolases (EC 3.5.1.-) contracted in NTF ($p = 1.87e-08$), with a mean value of 3.71 (SD = 0.76), compared to 11.24 (SD = 3.49) in non-NTF (fold change = 0.33, effect size r = 0.024) (Fig. S4 and Supplementary Table 12). These hydrolases are conserved among NTF (Fig. S4) belong to the nitrilase superfamily, which can break carbon–nitrogen bonds to degrade organic nitrogen compounds and produce ammonia (Pace and Brenner, 2001). Importantly, these contracted hydrolases may minimize nitrogen volatilization as ammonia, which is a critical adaptation for nitrogen retention in oligotrophic soils. In contrast, many more carbon–nitrogen hydrolase coding genes were identified in entomopathogens and nematode endoparasites, suggesting that they mainly utilize protein-derived nutrients for energy (Supplementary Table 12). The genes encoding amino acid permeases, which contribute to amino acid transport, are enriched in the NTF-specific OGs (Supplementary Table 7). This permease expansion likely enhanced the direct assimilation of nitrogen-rich metabolites from prey, bypassing energetically costly decomposition pathways. These patterns suggest that NTF evolved to utilize organic nitrogen more efficiently by contracting carbon–nitrogen hydrolase genes (to reduce the loss of nitrogen in the form of ammonia) and gaining specific amino acid permease genes (to assimilate nitrogen in nitrogen-poor environments), supporting the hypothesis that these genomic changes were selected to help NTF adapt to nitrogen-poor conditions.

3.3. Genome evolution putatively linked to carnivorism

NTF are expected to secrete numerous proteins that participate in capturing and consuming nematodes. We compared the predicted secreted proteins between NTF and non-NTF. The number of secreted proteins ranged from 284 to 1,654 (Fig. S5; Supplementary Tables 12 and 13). After normalization using the total number of genes for each genome, the ratio of secreted proteins encoded by NTF was significantly higher than that of non-NTF ($p = 1.07e-4$, Mann-Whitney U test, fold change = 1.32, effect size r = 17.86), suggesting an ancestral burst of the
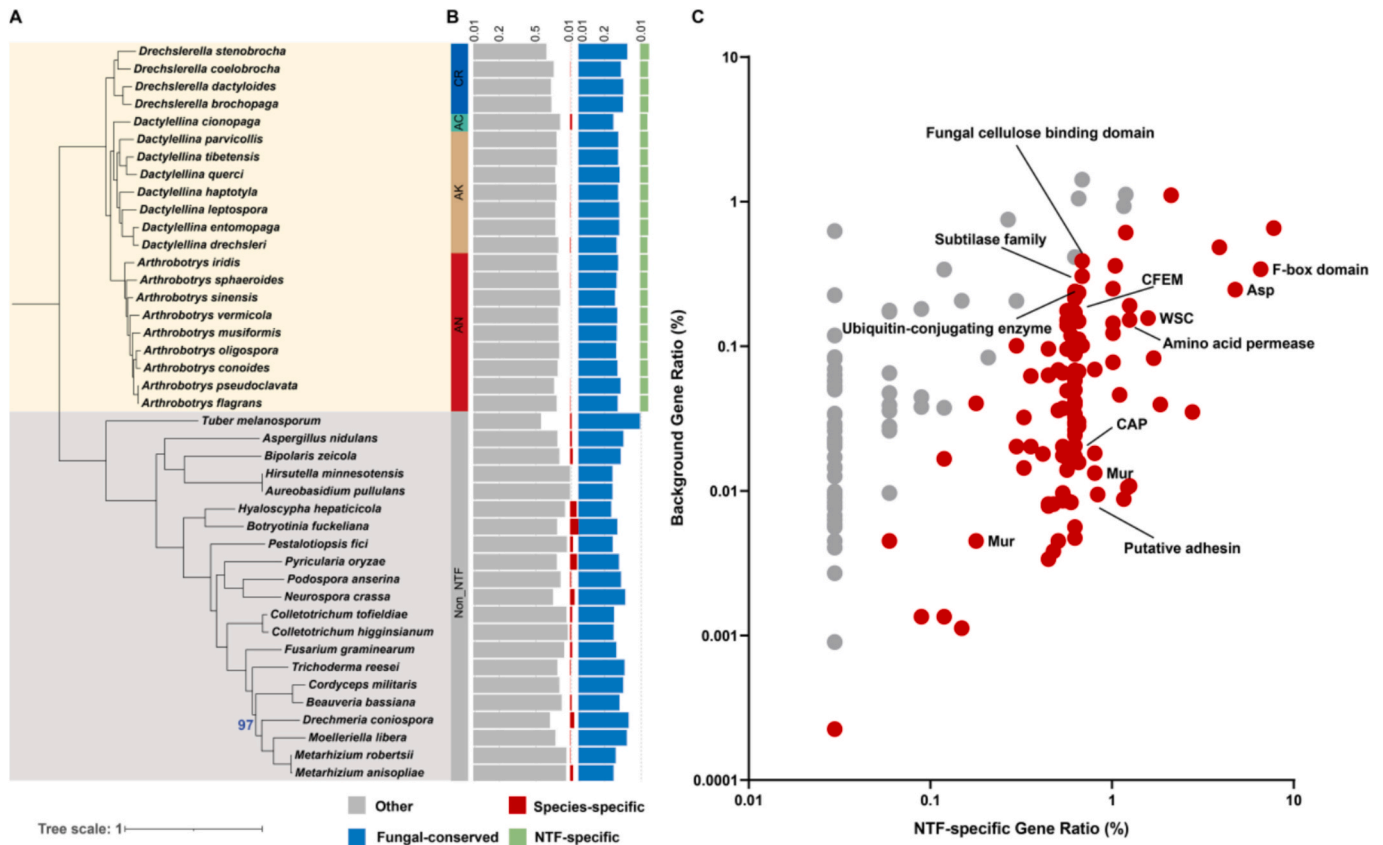
Fig. 1. Phylogenetic relationship of the species analyzed and characteristics of the genes in individual genomes. (A) Maximum likelihood phylogeny of 21 NTF (yellow background) and 21 non-NTF (gray background) constructed using protein sequences of 704 single-copy orthologous genes present in all species. The following color scheme was used to denote different trapping devices: green (adhesive columns, AC), gold (adhesive knobs, AK), red (adhesive nets, AN), and blue (constricting rings, CR). All bootstrap values were 100 unless otherwise indicated. (B) The bar chart shows the total number of protein-coding genes in each species. The genes were classified as fungal-conserved (blue), NTF-specific (green), species-specific (red), and those present only in some fungi (gray) based on OrthoFinder group. (C) The plot shows the distribution of Pfam domains among the NTF-specific genes. Each dot represented a gene illustrated by background gene ratio (%) and NTF-specific gene ratio (%) classified by Pfam domains. Enriched Pfam domains among the NTF-specific genes (see Dataset S1, Table S3) are highlighted in red ($p <$ 0.05, Mann-Whitney U test) and include those associated with nematode capture (CFEM domain (PF05730)), nematode infection and consumption (eukaryotic aspartyl protease (PF00026), subtilase family (PF00082) and cysteine-rich secretory protein family (PF00188)), and ubiquitination degradation of proteins such as F-box domain (PF00646), amino acid permease (PF00324) and ubiquitin-conjugating enzyme (PF00179). (For interpretation of the references to color in this figure legend, the reader is referred to the web version of this article.)

secreted protein repertoire.

The extracellular adhesive layer of traps is essential for nematode capture. Three types of adhesive proteins, including those containing GLEYA (PF10528), Egh16-like (PF11327), and CFEM (PF05730), were predicted to be involved in capturing nematodes (Ji et al., 2020; Liang et al., 2015; Zhang et al., 2020). These adhesive proteins accounted for more than 2 % of the secreted proteins in all NTF, which is higher than that in non-NTF (Fig. 4A; Supplementary Table 14). In addition, the ratios of GLEYA domains ($p <$ 0.0001, Mann-Whitney U test, fold change = 3.64, effect size r = 17.88) and Egh16-like domains ($p <$ 0.0001, Mann-Whitney U test, fold change = 5.49, effect size r = 20.74) in NTF are significantly higher than those in non-NTF. The CFEM domain is important in plant pathogenic fungi; therefore, despite being common in NTF, it was not statistically significant when comparing NTF and non-NTF. Gene expression patterns in three representative NTF (*Ar. oligospora*, *Da. haptotyla* and *Dr. dactyloides*) during nematode capture showed that the genes for 9.5 % (2/21) of the adhesive proteins with a GLEYA domain and 15.2 % (5/33) of the adhesive proteins with an Egh16-like domain were up-regulated (Supplementary Tables 15 and 17), supporting the hypothesis that expansion and up-regulation of adhesive protein-coding genes represent a genomic adaptation for a predatory lifestyle.

The nematode cuticle is a three-layered structure consisting mainly

of collagen and non-collagenous proteins. The CAP superfamily (PF00188), composed of cysteine-rich secretory proteins, antigen 5, and pathogenesis-related 1 proteins, expanded among NTF (Supplementary Table 9). This superfamily participates in reproduction, virulence, venom toxicity, cellular defense, and immune evasion (Darwiche et al., 2016; Gibbs et al., 2008). All three NTF analyzed showed that 36.4 % (4/11) of the CAP superfamily genes were up-regulated in the presence of nematodes (Supplementary Tables 15 and 18), suggesting their involvement in nematode infection. In addition, the genes for serine peptidases, which are involved in nematode consumption, also significantly expanded in NTF (Fig. 4B), and 15.6 % (10/64) of the genes encoding members of the subtilisin family in three NTF were up-regulated during predation (Supplementary Tables 15 and 19).

Fungi produce diverse secondary metabolites (SMs), some of which are "chemical weapons" against other organisms (Keller, 2018; Rohlfs and Churchill, 2011). Comparative analysis revealed that NTF possess significantly fewer and less conserved SM gene clusters compared to non-NTF species, although this could reflect metabolic trade-offs between specialized traits. However, similar to other Ascomycota fungi, individual SMs may be important for organismal ecology (Raffa and Keller, 2019; Steenwyk et al., 2020c). The number of predicted SM gene clusters ranged from 6 to 23 in NTF (mean of 13.14, fold change = 0.29, effect size r = 0.57), which is significantly lower than that of non-NTF:
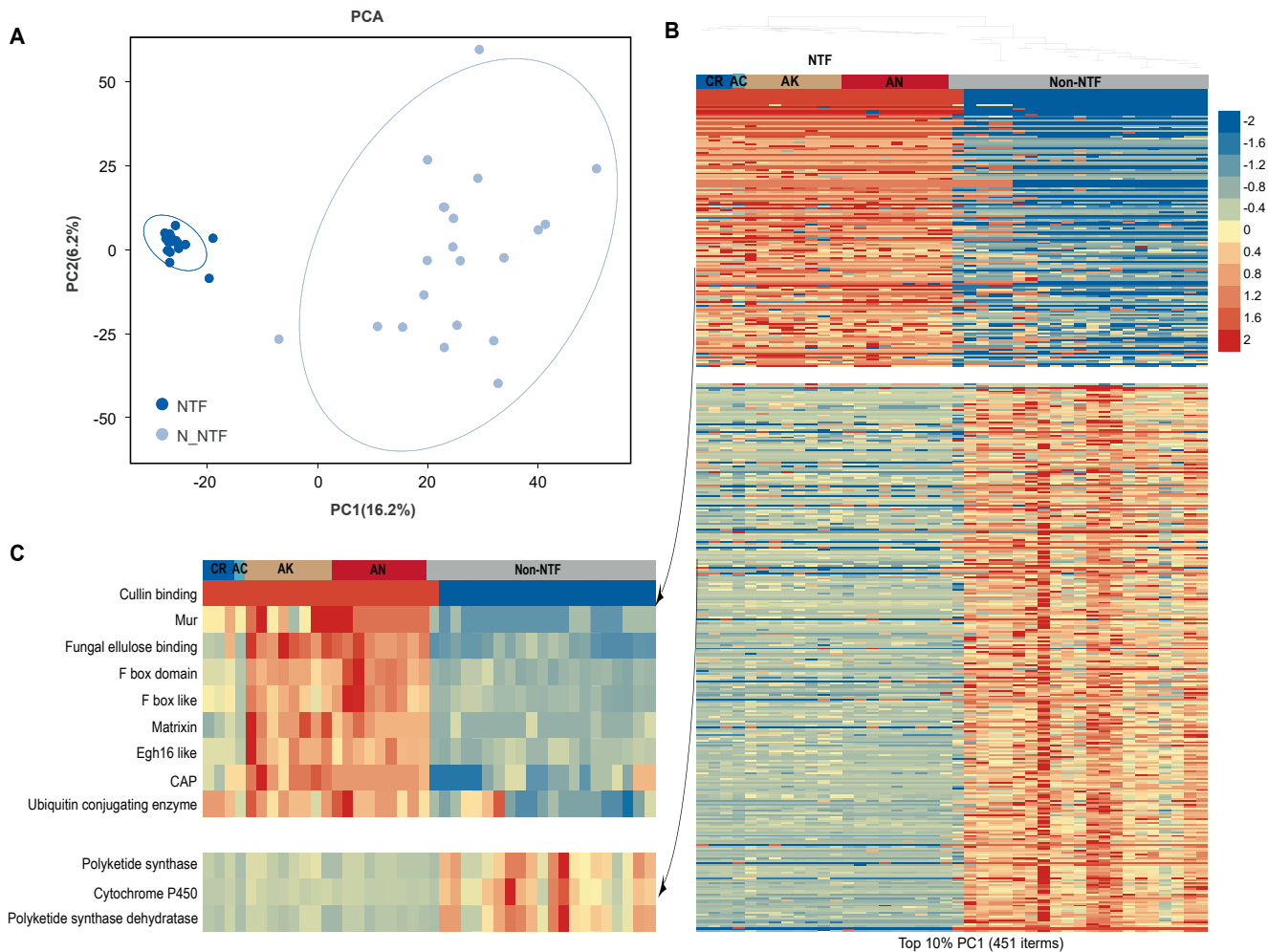
Fig. 2. Contrasting diversification of protein domains between NTF and non-NTF. (A) Principal component analysis (PCA) based on the presence and number of Pfam domains in multiple orthologous groups (OGs) across NTF and non-NTF. The first two principal components account for 16.2% and 6.2% of variation, respectively. The 21 NTF are clustered together according to PC1. **(B)** Heatmaps were compiled from the Pfam data that contributed most (top 10%, 451 items). Different patterns of Pfam domain expansion and contraction are seen between NTF (yellow background) and non-NTF (gray background) based on their normalized numbers. The following color scheme was used to denote different trapping devices: green (adhesive columns, AC), gold (adhesive knobs, AK), red (adhesive nets, AN), and blue (constricting rings, CR). **(C)** Heatmaps highlighting the candidate Pfam domains related to carnivorous lifestyle selected from those shown in panel **B**. (For interpretation of the references to color in this figure legend, the reader is referred to the web version of this article.)

endophytic and phytopathogenic fungi (mean of 49.42, $p < 0.0001$) and entomopathogenic and nematode-endoparasitic fungi (mean of 59.29, $p < 0.0001$) (Fig. 4C; Supplementary Table 20). Only *T. melanosporum*, a mutualistic ectomycorrhizal fungus, has 9 clusters. While, the polyketide synthase (PKS) gene clusters are not conserved among NTF, suggesting lineage-specific roles for these SMs.

Non-vertical evolution, including HGT, has been instrumental in driving the rapid adaptive evolution of fungi and has played a role in the emergence of new pathogens (Feurtey and Stukenbrock, 2018; Steenwyk et al., 2020b). Among the 89 potential HGT events observed in NTF, the HGT of *Mur* genes, which are involved in bacterial cell wall biosynthesis (Radkov et al., 2018), is notable. Top 100 BLASTp results obtained using *Ar. oligospora* proteins revealed that 4 proteins with Mur domains were highly similar to MurA (53.1–69.2 % identity; 90–96 % coverage), MurC (65.8–72 % identity; 98–99 % coverage), MurD (63.7–70.2 % identity; 98–99 % coverage), and MurE (39.2–49.4 % identity; 92–98 % coverage), respectively. Maximum-likelihood phylogenetic trees were constructed using RAxML (Fig. 5A, Fig. S6). The *MurE* gene was found in all NTF, suggesting its horizontal transfer before NTF diversification. The presence of introns in the NTF *MurE* gene indicates that the gene underwent eukaryotization. The function of NTF *MurE* in carnivorism was studied by disrupting the gene in *Dr. dactyloides*.

Compared with the wild type, three independently isolated mutants showed a reduced ability to attract *C. elegans* ($p = 1.1e-4$, 2.5e-3, 5.2e-4, two-tailed *t*-test, n = 5), with the attraction indices of the mutants being only 36.0 % of that of the wild type (Fig. 5B).

Analysis using CLEAN (contrastive learning-enabled enzyme annotation), which predicts enzyme function (Gregoire et al., 2023), showed that one NTF-specific OG with the polysaccharide lyase family 8 domain is closely related to Hyl, a bacterial hyaluronate lyase (EC:4.2.2.1). Hyl is an important virulence factor employed by Gram-positive bacteria to enhance their infectivity by degrading extracellular hyaluronate and chondroitin sulfate of animal hosts (Patil et al., 2023). All NTF species encode two Hyl homologs, except for *Dr. stenobrocha* (one homolog). The maximum-likelihood phylogenetic tree of this OG showed that the two homologs belong to distinct clades (Fig. S7), suggesting that they may have originated from different bacteria through two separate HGT events. Bacterial hyaluronate lyases are typically secreted; however, their NTF homologs lack a signal peptide. Most of one Hy1 clade have putative transmembrane domains, whereas those in the other clade lack transmembrane domains (Fig. S7). Further studies are required to determine whether Hyl homologs contribute to nematode carnivorism.
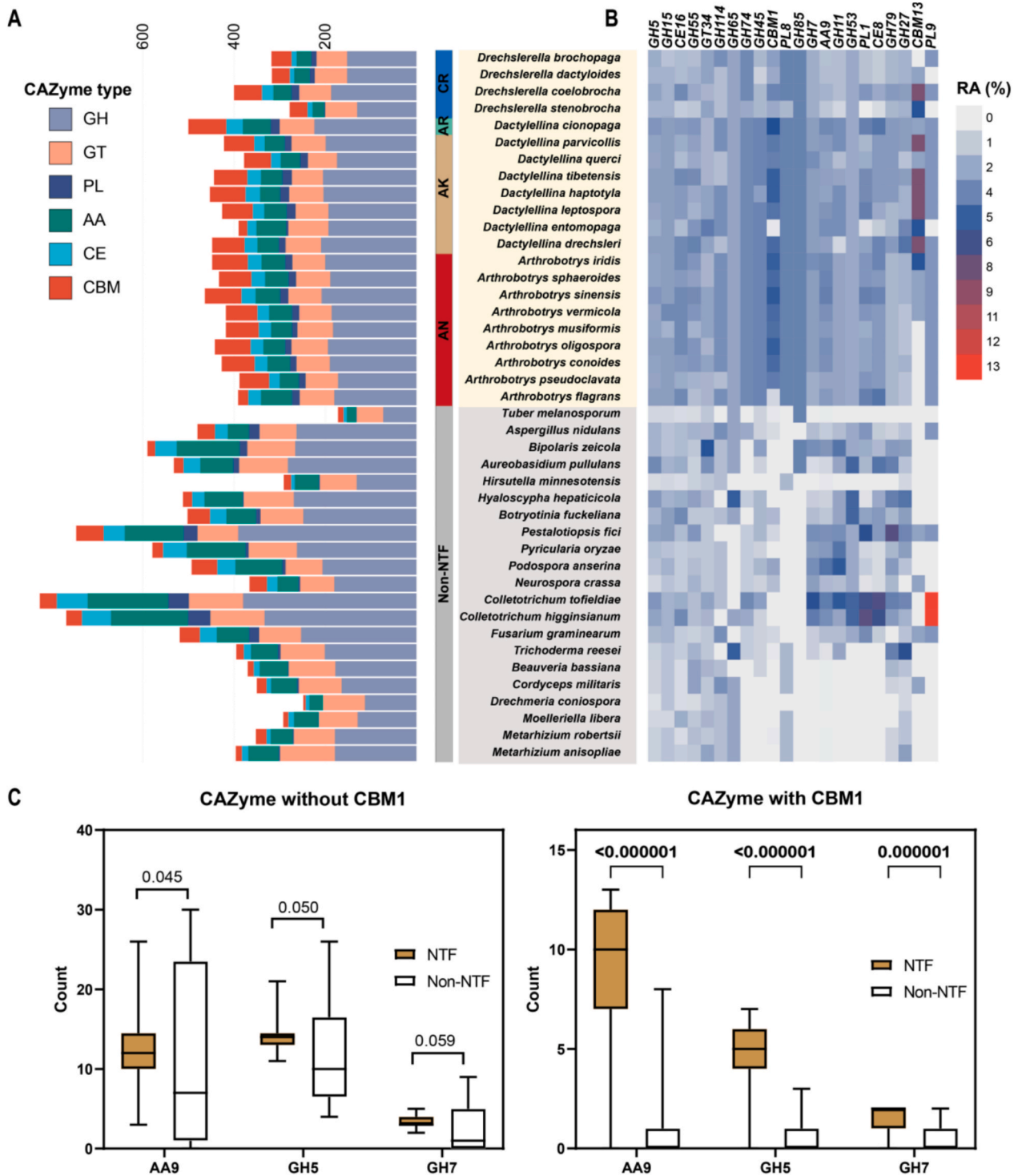
Fig. 3. Comparative analysis of the CAZymes among NTF and non-NTF. (**A**) The bar chart shows the numbers of the following CAZymes encoded by 21 NTF (yellow background) and 21 non-NTF (gray background): glycoside hydrolases (GH), glycosyl transferases (GT), carbohydrate esterases (CE), polysaccharide lyases (PL), auxiliary activities (AA), and carbohydrate-binding modules (CBM). The following color scheme was used to denote different trapping devices: green (adhesive columns, AC), gold (adhesive knobs, AK), red (adhesive nets, AN), and blue (constricting rings, CR). (**B**) Relative abundance (RA) profiles of 13 GHs, 2 GTs, 2 CBMs, 3 PLs, 1 AAs, and 2 CEs involved in degrading cellulose. The gene number for each class was divided by the total gene number. (**C**) Comparison of the numbers of cellulose degrading enzymes with or without CBM1 between NTF (light brown) and non-NTF (white) using Mann-Whitney *U* test (*p*-values are shown on the graphs). The numbers of AA9, GH5, and GH7 without CBM1 (left) or with CBM1 (right) are presented. (For interpretation of the references to color in this figure legend, the reader is referred to the web version of this article.)
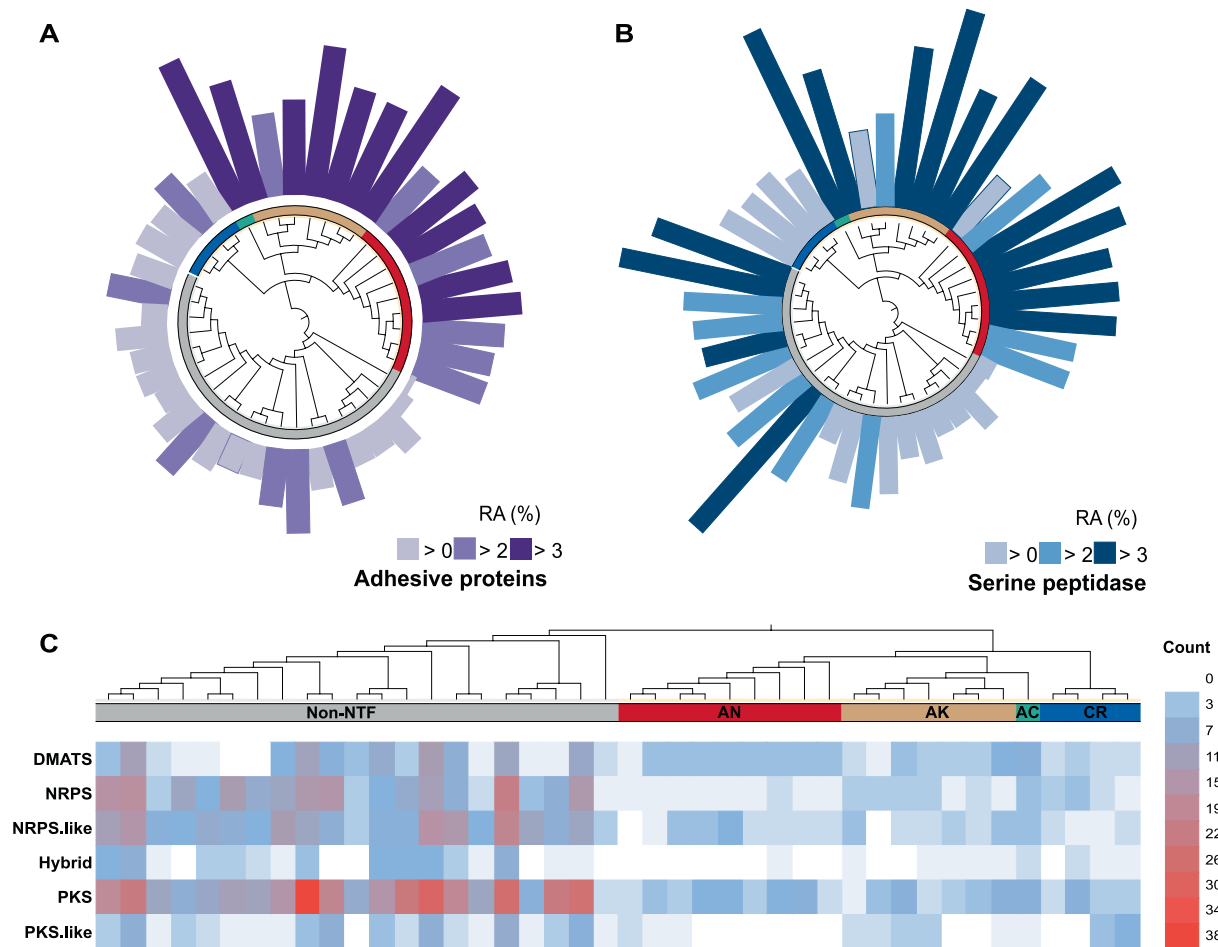
Fig. 4. Distribution patterns of adhesive proteins, serine peptidases, and secondary metabolism clusters among NTF and non-NTF. The following color schemes were used to denote different trapping devices: blue (constricting rings, CR), red (adhesive nets, AN), green (adhesive columns, AC), and gold (adhesive knobs, AK). (**A**, **B**) Relative abundance (RA) of adhesive proteins (**A**) and serine peptidases (**B**) among the total secreted proteins encoded by each species. The numbers of adhesive proteins and serine peptidases were divided by the total number of secreted proteins to calculate their RA. (**C**) A heatmap shows the numbers of different types of secondary metabolism gene clusters in each species. (For interpretation of the references to color in this figure legend, the reader is referred to the web version of this article.)

4. Discussion

Approximately 5 million years after the Permian-Triassic mass extinction event, the global ecosystem stabilized and underwent extensive remodeling during the process (Ezcurra and Butler, 2018; Rampino et al., 2020). Ecosystems faced accelerated organic matter accumulation (Visscher et al., 1996), whereas nitrogen cycling shifted to ammonium-dominated states because of nitrate depletion (Romano et al., 2013; Sun et al., 2019). These carbon-rich but nitrogen-poor conditions set the stage for biotic recovery, as evidenced by a sharp increase in the biomass and diversity of taxa, including fungi, algae, and ferns, in the immediate aftermath of plant collapse in the late Permian (Mays et al., 2020). The availability of new niches resulting from this mass extinction event likely accelerated innovation during the recovery period (Lowery and Fraass, 2019).

The lifestyle of the fungi that gave rise to NTF after mass extinction remains unclear. In this study, we identified multiple genome changes—gene family gain/loss and HGT—that are associated with the evolution of NTF ecology and carnivorous lifestyles (Fig. 6). For example, gene families that have been reported to play critical roles in trap morphogenesis (Yang et al., 2020, 2018; Zhang et al., 2021), such as components of the G-protein mediated signaling and ubiquitin-conjugating enzyme Ubr1 (Supplementary Table 9), have expanded. Similarly, the genes of cell-surface proteins containing the

carbohydrate-binding WSC domain were up-regulated during nematode infection (Andersson et al., 2013, 2014) and were found to be significantly expanded in NTF (Supplementary Table 9). Other expanded gene families that may be linked to fungal carnivorism are those encoding adhesive proteins and proteases such as subtilase (Ji et al., 2020; Liang et al., 2015; Wang et al., 2015; Zhang et al., 2020). The patterns of gene family expansion in NTF resemble those observed in plant pathogens rather than patterns found in insect and animal pathogens (Meerupati et al., 2013). NTF show expansions in gene families related to carbohydrate metabolism, adhesion, and proteases, aligning with the strategies of plant pathogens for degrading host cell walls and obtaining nutrients. In contrast, NTF differ from insect pathogens such as *Metarhizium* species because they did not prioritize expansions in chitinases, toxin-related genes, or oxidative stress response proteins, highlighting the specialization of NTF in nematode predation. The evolution of various trapping devices by fungi to capture nematodes as a nitrogen source was hypothesized to be an innovation crucial for NTF (Yang et al., 2012). Here we found two changes that helped optimize this mode of nitrogen acquisition. Carbon-nitrogen hydrolase genes were reduced among NTF, a change that may enhance nitrogen retention by reducing the decomposition of organic nitrogen compounds to ammonia. Meanwhile, genes for specific amino acid permeases expanded in NTF. Some class III aminotransferase genes, which help enhance nitrogen assimilation, are up-regulated during nematode capturing (Supplementary
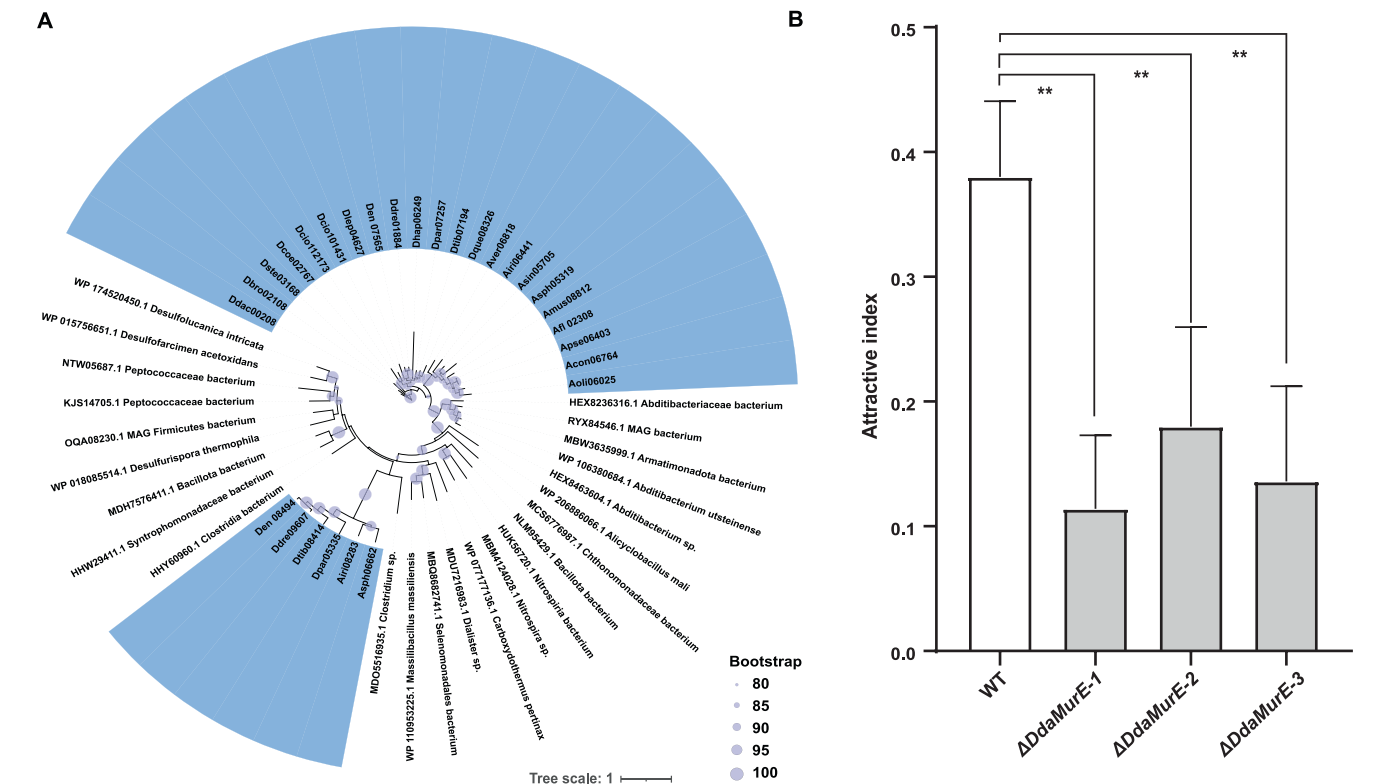
Fig. 5. The phylogenetic relationship and potential function of *MurE*. (A) Unrooted maximum-likelihood trees based on *MurE* protein sequences were constructed using RAxML. The bacterial species (only one genome sequence selected for each species) included were chosen based on the top 100 BLASTp results with the corresponding *Arthrobotrys oligospora* protein sequences as queries. All NTF species included in blue background. (B) Attractive indexes of *Drechslerella dactyloides* wild type (WT) strain and three *ΔDdaMurE* mutants on water agar (WA) medium. **$p < 0.01$, two-tailed *t*-test, n = 5. (For interpretation of the references to color in this figure legend, the reader is referred to the web version of this article.)
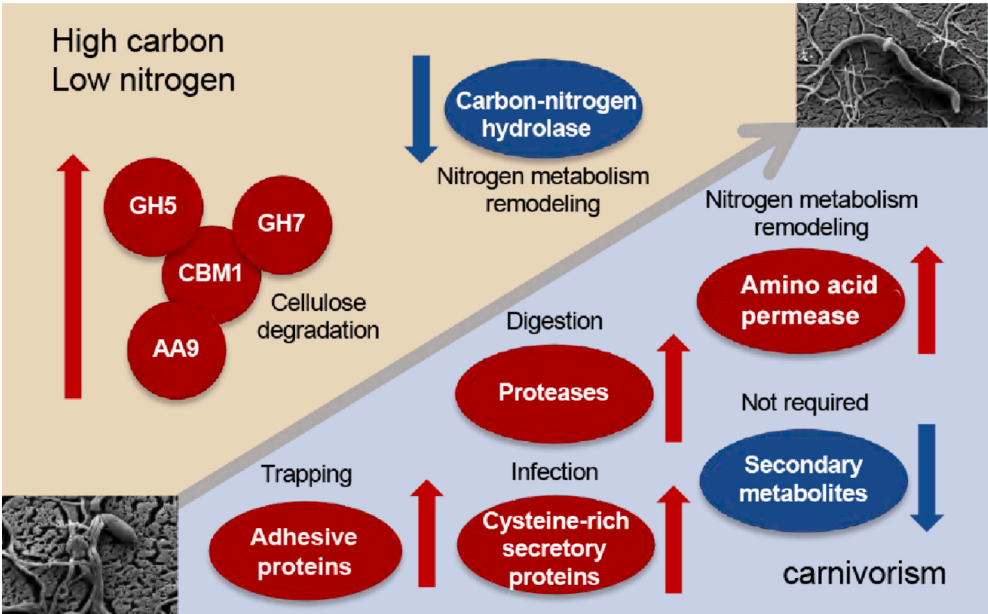
Fig. 6. Proposed model for genomic changes associated with the evolution of NTF. To adapt to carbon-rich/nitrogen-poor environments, the genes for amino acid permease and cellulose degradation enzymes expanded, whereas the genes for carbon–nitrogen hydrolase contracted. The genes encoding adhesive proteins, cysteine-rich secretory proteins, and proteases, which are likely involved in nematode capture, infection, and consumption, respectively, were expanded to support carnivorism. The number of secondary metabolite gene clusters was significantly reduced.

Table 16). These patterns suggest that NTF evolved to recycle nitrogen resources efficiently by remodeling their nitrogen metabolism.

Perhaps most strikingly, NTF have horizontally acquired multiple *Mur* genes, which are involved in bacterial cell wall peptidoglycan synthesis, from bacteria to ensnare nematodes. Phylogenetic analysis revealed that the constituents of the *Mur* gene cluster were acquired

through multiple complex HGT events (Fig. 5A and S3). Gene clusters originating from multiple HGT events have been observed in Saccharomycotina yeast (Gonçalves and Gonçalves, 2019), and our analyses suggest that this may be a more widespread phenomenon in fungi. Nematodes consume bacteria as food and have chemotaxis to bacteria, while NTF attract nematodes to capture. Disruption of the *MurE* gene reduced nematode attraction (Fig. 5B), suggesting the involvement of the *Mur* genes in nematode attraction. N-acetylglucosamine (GlcNAc) serves as a precursor for chitin synthesis in fungi and peptidoglycan synthesis in bacteria. The *Mur* genes in NTF—originally involved in bacterial peptidoglycan biosynthesis—may repurpose GlcNAc metabolism to modify trap-specific cell wall components. The cell wall of the nematode traps appeared different from that of the hyphae (Fig. S8).

Our study uncovered multiple modes of genomic changes that likely influenced the evolutionary trajectory of NTF, implicating several gene families that have previously been shown to be linked to the NTF lifestyle (Fig. 6). More importantly, our comprehensive analysis identified novel candidate genes and evolutionary processes that might underlie specific stages of predation, such as attraction and consumption. Integrated analysis of the transcriptomic dataset provided preliminary validation of predation-associated expression patterns for these candidate genes, although definitive mechanistic confirmation through targeted approaches (e.g., gene knockouts and heterologous expression) remains essential. A notable challenge lies in the high proportion of orphan genes (65.4 % of NTF-specific OGs) that lack functional annotation, underscoring the need for systematic functional characterization to uncover their potential roles in carnivory. Taken together, our work established an extensive genome resource and ample hypotheses that will guide future studies to understand the origins and evolution of NTF and to confirm the involvement of candidate genes associated with NTF lifestyles.

Data availability

Data from the whole genome shotgun sequencing of 16 NTF reported in this paper are available at GenBank under the BioProject number PRJNA791178 (https://www.ncbi.nlm.nih.gov/bioproject/791178). Corresponding accession numbers are JAJTUI000000000 (*Arthrobotrys conoides*), JAJTTS000000000 (*A. iridis*), JAJTTT000000000 (*A. musiformis*), JAJTTU000000000 (*A. pseudoclavata*), JAJTTV000000000 (*A. sinensis*), JAJTTW000000000 (*A. sphaeroides*), JAJTTX000000000 (*A. vermicola*), JAJTTY000000000 (*Dactylellina cionopaga*), JAJTUB000000000 (*D. drechsleri*), JAJTUC000000000 (*D. leptospora*), JAJTUD000000000 (*D. parvicollis*), JAJTUE000000000 (*D. querci*), JAKDFA000000000 (*D. tibetensis*), JAJTUF000000000 (*Drechslerella brochopaga*), JAJTUH000000000 (*Dr. coelobrocha*), and JAJTUG000000000 (*Dr. dactyloides*).

CRediT authorship contribution statement

Yani Fan: Writing – review & editing, Writing – original draft, Methodology, Investigation, Conceptualization. **Minghao Du:** Visualization, Software, Investigation, Conceptualization. **Weiwei Zhang:** Methodology, Investigation, Data curation, Conceptualization. **Wei Deng:** Writing – review & editing, Visualization, Investigation. **Ence Yang:** Writing – review & editing, Methodology, Formal analysis. **Shunxian Wang:** Methodology, Investigation. **Luwen Yan:** Methodology, Investigation. **Liao Zhang:** Investigation, Data curation. **Seogchan Kang:** Writing – review & editing. **Jacob L Steenwyk:** Writing – review & editing, Software. **Zhiqiang An:** Writing – review & editing, Conceptualization. **Xingzhong Liu:** Writing – review & editing, Resources, Project administration, Funding acquisition, Data curation, Conceptualization. **Meichun Xiang:** Methodology, Conceptualization.

Declaration of competing interest

Acknowledgments

Appendix A. Supplementary material

Supplementary data to this article can be found online at https://doi.org/10.1016/j.ympev.2025.108423.

References

Almagro Armenteros, J.J., Tsirigos, K.D., Sønderby, C.K., Petersen, T.N., Winther, O., Brunak, S., von Heijne, G., Nielsen, H., 2019. SignalP 5.0 improves signal peptide predictions using deep neural networks. Nat. Biotechnol. 37, 420–423. https://doi.org/10.1038/S41587-019-0036-Z.

Andersson, K.M., Kumar, D., Bentzer, J., Friman, E., Ahrén, D., Tunlid, A., 2014. Interspecific and host-related gene expression patterns in nematode-trapping fungi. BMC Genomics 15, 968. https://doi.org/10.1186/1471-2164-15-968.

Andersson, K.M., Meerupati, T., Levander, F., Friman, E., Ahrén, D., Tunlida, A., 2013. Proteome of the nematode-trapping cells of the fungus *Monacrosporium haptotylum*. Appl. Environ. Microbiol. 79, 4993–5004. https://doi.org/10.1128/AEM.01390-13.

Armenteros, J.J.A., Salvatore, M., Emanuelsson, O., Winther, O., Von Heijne, G., Elofsson, A., Nielsen, H., 2019. Detecting sequence signals in targeting peptides using deep learning. Life Sci. Alliance 2, e201900429. https://doi.org/10.26508/lsa.201900429.

Bajic, D., Sanchez, A., 2020. The ecology and evolution of microbial metabolic strategies. Curr. Opin. Biotechnol. 62, 123–128. https://doi.org/10.1016/J.COPBIO.2019.09.003.

Barron, G.L., 2003. Predatory fungi, wood decay, and the carbon cycle. Biodiversity 4, 3–9. https://doi.org/10.1080/14888386.2003.9712621.

Barron, G.L., 1992. Lignolytic and cellulolytic fungi as predators and parasites. In: Garroll, G.C., Wicklow, D.T. (Eds.), The Fungal Community: Its Organization and Role in the Ecosystem. Routledge, Abingdon, pp. 311–326.

Benton, M.J., Twichett, R.J., 2003. How to kill (almost) all life: the end-Permian extinction event. Trends Ecol. Evol. 18, 358–365. https://doi.org/10.1016/S0169-5347(03)00093-4.

Blackburn, T.J., Olsen, P.E., Bowring, S.A., McLean, N.M., Kent, D.V., Puffer, J., McHone, G., Rasbury, E.T., Et-Touhami, M., 2013. Zircon U-Pb geochronology links the end-Triassic extinction with the central Atlantic magmatic Province. Science 340, 941–945. https://doi.org/10.1126/science.1234204.

Boetzer, M., Henkel, C.V., Jansen, H.J., Butler, D., Pirovano, W., 2011. Scaffolding pre-assembled contigs using SSPACE. Bioinformatics 27, 578–579. https://doi.org/10.1093/BIOINFORMATICS/BTQ683.

Bolger, A.M., Lohse, M., Usadel, B., 2014. Trimmomatic: a flexible trimmer for Illumina sequence data. Bioinformatics 30, 2114–2120. https://doi.org/10.1093/BIOINFORMATICS/BTU170.

Capella-Gutiérrez, S., Silla-Martínez, J.M., Gabaldón, T., 2009. trimAl: a tool for automated alignment trimming in large-scale phylogenetic analyses. Bioinformatics 25, 1972–1973. https://doi.org/10.1093/BIOINFORMATICS/BTP348.

Chundawat, S.P.S., Nemmaru, B., Hackl, M., Brady, S.K., Hilton, M.A., Johnson, M.M., Chang, S., Lang, M.J., Huh, H., Lee, S.H., Yarbrough, J.M., López, C.A., Gnanakaran, S., 2021. Molecular origins of reduced activity and binding commitment of processive cellulases and associated carbohydrate-binding proteins to cellulose III. J. Biol. Chem. 296, 100431. https://doi.org/10.1016/J.JBC.2021.100431.

Darwiche, R., Kelleher, A., Hudspeth, E.M., Schneiter, R., Asojo, O.A., 2016. Structural and functional characterization of the CAP domain of pathogen-related yeast 1 (Pry1) protein. Sci. Rep. 6, 28838. https://doi.org/10.1038/SREP28838.

Emms, D.M., Kelly, S., 2019. OrthoFinder: phylogenetic orthology inference for comparative genomics. Genome Biol. 20, 238. https://doi.org/10.1186/S13059-019-1832-Y.

Espagne, E., Lespinet, O., Malagnac, F., Da Silva, C., Jaillon, O., Porcel, B.M., Couloux, A., Aury, J.M., Ségurens, B., Poulain, J., Anthouard, V., Grossetete, S., Khalili, H., Coppin, E., Déquard-Chablat, M., Picard, M., Contamine, V., Arnaise, S.,

Bourdais, A., Berteaux-Lecellier, V., Gautheret, D., de Vries, R.P., Battaglia, E., Coutinho, P.M., Danchin, E.G., Henrissat, B., Khoury, R.E., Sainsard-Chanet, A., Boivin, A., Pinan-Lucarré, B., Sellem, C.H., Debuchy, R., Wincker, P., Weissenbach, J., Silar, P., 2008. The genome sequence of the model ascomycete fungus *Podospora anserina*. Genome Biol. 9, 1–22. https://doi.org/10.1186/GB-2008-9-5-R77/FIGURES/7.

Ezcurra, M.D., Butler, R.J., 2018. The rise of the ruling reptiles and ecosystem recovery from the Permo-Triassic mass extinction. Proc. Biol. Sci. 285, 20180361. https://doi.org/10.1098/RSPB.2018.0361.

Fan, Y., Zhang, W., Chen, Y., Xiang, M., Liu, X., 2021. DdaSTE12 is involved in trap formation, ring inflation, conidiation, and vegetative growth in the nematode-trapping fungus *Drechslerella dactyloides*. Appl. Microbiol. Biotechnol. 105, 7379–7393. https://doi.org/10.1007/S00253-021-11455-Z.

Feurtey, A., Stukenbrock, E.H., 2018. Interspecific gene exchange as a driver of adaptive evolution in fungi. Annu. Rev. Microbiol. 72, 377–398. https://doi.org/10.1146/ANNUREV-MICRO-090817-062753.

Floudas, D., Binder, M., Riley, R., Barry, K., Blanchette, R.A., Henrissat, B., Martínez, A. T., Otillar, R., Spatafora, J.W., Yadav, J.S., Aerts, A., Benoit, I., Boyd, A., Carlson, A., Copeland, A., Coutinho, P.M., De Vries, R.P., Ferreira, P., Findley, K., Foster, B., Gaskell, J., Glotzer, D., Górecki, P., Heitman, J., Hesse, C., Hori, C., Igarashi, K., Jurgens, J.A., Kallen, N., Kersten, P., Kohler, A., Kües, U., Kumar, T.K.A., Kuo, A., LaButti, K., Larrondo, L.F., Lindquist, E., Ling, A., Lombard, V., Lucas, S., Lundell, T., Martin, R., McLaughlin, D.J., Morgenstern, I., Morin, E., Murat, C., Nagy, L.G., Nolan, M., Ohm, R.A., Patyshakuliyeva, A., Rokas, A., Ruiz-Dueñas, F.J., Sabat, G., Salamov, A., Samejima, M., Schmutz, J., Slot, J.C., John, F.S., Stenlid, J., Sun, H., Sun, S., Syed, K., Tsang, A., Wiebenga, A., Young, D., Pisabarro, A., Eastwood, D.C., Martin, F., Cullen, D., Grigoriev, I.V., Hibbett, D.S., 2012. The Paleozoic origin of enzymatic lignin decomposition reconstructed from 31 fungal genomes. Science 336, 1715–1719. https://doi.org/10.1126/SCIENCE.1221748.

Gibbs, G.M., Roelants, K., O'Bryan, M.K., 2008. The CAP superfamily: cysteine-rich secretory proteins, antigen 5, and pathogenesis-related 1 proteins–roles in reproduction, cancer, and immune defense. Endocr. Rev. 29, 865–897. https://doi.org/10.1210/ER.2008-0032.

Gnerre, S., MacCallum, I., Przybylski, D., Ribeiro, F.J., Burton, J.N., Walker, B.J., Sharpe, T., Hall, G., Shea, T.P., Sykes, S., Berlin, A.M., Aird, D., Costello, M., Daza, R., Williams, L., Nicol, R., Gnirke, A., Nusbaum, C., Lander, E.S., Jaffe, D.B., 2011. High-quality draft assemblies of mammalian genomes from massively parallel sequence data. PNAS 108, 1513–1518. https://doi.org/10.1073/PNAS.1017351108.

Gonçalves, C., Gonçalves, P., 2019. Multilayered horizontal operon transfers from bacteria reconstruct a thiamine salvage pathway in yeasts. PNAS 116, 22219–22228. https://doi.org/10.1073/pnas.1909844116.

Gregoire, J.M., Zhou, L., Haber, J.A., 2023. Combinatorial synthesis for AI-driven materials discovery. Nat Synthesis 2, 493–504. https://doi.org/10.1038/s44160-023-00251-4.

Hoff, K.J., Lange, S., Lomsadze, A., Borodovsky, M., Stanke, M., 2016. BRAKER1: unsupervised RNA-Seq-based genome annotation with GeneMark-ET and AUGUSTUS. Bioinformatics 32, 767–769. https://doi.org/10.1093/BIOINFORMATICS/BTV661.

Horton, P., Park, K.J., Obayashi, T., Fujita, N., Harada, H., Adams-Collier, C.J., Nakai, K., 2007. WoLF PSORT: protein localization predictor. Nucleic Acids Res. 35. https://doi.org/10.1093/NAR/GKM259.

Ji, X., Yu, Z., Yang, J., Xu, J., Zhang, Y., Liu, S., Zou, C., Li, J., Liang, L., Zhang, K.Q., 2020. Expansion of adhesion genes drives pathogenic adaptation of nematode-trapping fungi. iScience 23, 101057. https://doi.org/10.1016/J.ISCI.2020.101057.

Jones, P., Binns, D., Chang, H.Y., Fraser, M., Li, W., McAnulla, C., McWilliam, H., Maslen, J., Mitchell, A., Nuka, G., Pesseat, S., Quinn, A.F., Sangrador-Vegas, A., Scheremetjew, M., Yong, S.Y., Lopez, R., Hunter, S., 2014. InterProScan 5: genome-scale protein function classification. Bioinformatics 30, 1236–1240. https://doi.org/10.1093/BIOINFORMATICS/BTU031.

Kalyaanamoorthy, S., Minh, B.Q., Wong, T.K.F., von Haeseler, A., Jermiin, L.S., 2017. ModelFinder: fast model selection for accurate phylogenetic estimates. Nat. Methods 14, 587–589. https://doi.org/10.1038/nmeth.4285.

Katoh, K., Standley, D.M., 2013. MAFFT Multiple Sequence Alignment Software Version 7: Improvements in Performance and Usability. Mol. Biol. Evol. 30, 772–780. https://doi.org/10.1093/MOLBEV/MST010.

Keller, N.P., 2018. Fungal secondary metabolism: regulation, function and drug discovery. Nat. Rev. Microbiol. 17, 167–180. https://doi.org/10.1038/s41579-018-0121-1.

Khaldi, N., Seifuddin, F.T., Turner, G., Haft, D., Nierman, W.C., Wolfe, K.H., Fedorova, N. D., 2010. SMURF: Genomic mapping of fungal secondary metabolite clusters. Fungal Genet. Biol. 47, 736–741. https://doi.org/10.1016/J.FGB.2010.06.003.

Klosterman, S.J., Subbarao, K.V., Kang, S., Veronese, P., Gold, S.E., Thomma, B.P.H.J., Chen, Z., Henrissat, B., Lee, Y.H., Park, J., Garcia-Pedrajas, M.D., Barbara, D.J., Anchieta, A., de Jonge, R., Santhanam, P., Maruthachalam, K., Atallah, Z., Amyotte, S.G., Paz, Z., Inderbitzin, P., Hayes, R.J., Heiman, D.I., Young, S., Zeng, Q., Engels, R., Galagan, J., Cuomo, C.A., Dobinson, K.F., Ma, L.J., 2011. Comparative genomics yields insights into niche adaptation of plant vascular wilt pathogens. PLoS Pathog. 7, e1002137. https://doi.org/10.1371/JOURNAL.PPAT.1002137.

Kolde, R., 2019. pheatmap: Pretty Heatmaps. CRAN. https://cran.r-project.org/web/packages/pheatmap.

Krogh, A., Larsson, B., Von Heijne, G., Sonnhammer, E.L.L., 2001. Predicting transmembrane protein topology with a hidden Markov model: application to complete genomes. J. Mol. Biol. 305, 567–580. https://doi.org/10.1006/JMBI.2000.4315.

Le Saux, R., Quénéhervé, P., 2002. Differential chemotactic responses of two plant-parasitic nematodes, *Meloidogyne incognita* and *Rotylenchulus reniformis*, to some

inorganic ions. Nematology 4, 99–105. https://doi.org/10.1163/156854102760082258.

Lee, C.H., Chang, H.W., Yang, C.T., Wali, N., Shie, J.J., Hsueh, Y.P., 2020. Sensory cilia as the Achilles heel of nematodes when attacked by carnivorous mushrooms. PNAS 117, 6014–6022. https://doi.org/10.1073/PNAS.1918473117.

Li, Y., Hyde, K.D., Jeewon, R., Cai, L., Vijaykrishna, D., Zhang, K., 2005. Phylogenetics and evolution of nematode-trapping fungi (Orbiliales) estimated from nuclear and protein coding genes. Mycologia 97, 1034–1046. https://doi.org/10.3852/MYCOLOGIA.97.5.1034.

Li, Y., Steenwyk, J.L., Chang, Y., Wang, Y., James, T.Y., Stajich, J.E., Spatafora, J.W., Groenewald, M., Dunn, C.W., Hittinger, C.T., Shen, X.X., Rokas, A., 2021. A genome-scale phylogeny of the kingdom Fungi. Curr. Biol. 31, 1653–1665.e5. https://doi.org/10.1016/J.CUB.2021.01.074.

Liang, L., Shen, R., Mo, Y., Yang, J., Ji, X., Zhang, K.Q., 2015. A proposed adhesin AoMad1 helps nematode-trapping fungus *Arthrobotrys oligospora* recognizing host signals for life-style switching. Fungal Genet. Biol. 81, 172–181. https://doi.org/10.1016/J.FGB.2015.02.012.

Liu, K., Zhang, W., Lai, Y., Xiang, M., Wang, X., Zhang, X., Liu, X., 2014. *Drechslerella stenobrocha* genome illustrates the mechanism of constricting rings and the origin of nematode predation in fungi. BMC Genomics 15, 114. https://doi.org/10.1186/1471-2164-15-114.

Lopez-Llorca, L.V., Maciá-Vicente, J.G., Jansson, H.B., 2007. Mode of action and interactions of nematophagous fungi, in: Ciancio, A., Mukerji, K.G. (Eds.), Integrated Management and Biocontrol of Vegetable and Grain Crops Nematodes. Springer, Dordrecht, pp. 51–76.

Lowery, C.M., Fraass, A.J., 2019. Morphospace expansion paces taxonomic diversification after end cretaceous mass extinction. Nat. Ecol. Evol. 3, 900–904. https://doi.org/10.1038/S41559-019-0835-0.

Malar, C.M., Krüger, M., Krüger, C., Wang, Y., Stajich, J.E., Keller, J., Chen, E.C.H., Yildirir, G., Villeneuve-Laroche, M., Roux, C., Delaux, P.M., Corradi, N., 2021. The genome of *Geosiphon pyriformis* reveals ancestral traits linked to the emergence of the arbuscular mycorrhizal symbiosis. Curr. Biol. 31, 1570–1577.e4. https://doi.org/10.1016/J.CUB.2021.01.058.

Mays, C., Vajda, V., Frank, T.D., Fielding, C.R., Nicoll, R.S., Tevyaw, A.P., McLoughlin, S., 2020. Refined Permian–Triassic floristic timeline reveals early collapse and delayed recovery of south polar terrestrial ecosystems. GSA Bull. 132, 1489–1513. https://doi.org/10.1130/B35355.1.

Meerupati, T., Andersson, K.M., Friman, E., Kumar, D., Tunlid, A., Ahrén, D., 2013. Genomic mechanisms accounting for the adaptation to parasitism in nematode-trapping fungi. PLoS Genet. 9, e1003909. https://doi.org/10.1371/JOURNAL.PGEN.1003909.

Minh, B.Q., Schmidt, H.A., Chernomor, O., Schrempf, D., Woodhams, M.D., von Haeseler, A., Lanfear, R., 2020. IQ-TREE 2: New models and efficient methods for phylogenetic inference in the genomic era. Mol. Biol. Evol. 37, 1530–1534. https://doi.org/10.1093/molbev/msaa015.

Möller, E.M., Bahnweg, G., Sandermann, H., Geiger, H.H., 1992. A simple and efficient protocol for isolation of high molecular weight DNA from filamentous fungi, fruit bodies, and infected plant tissues. Nucleic Acids Res. 20, 6115–6116. https://doi.org/10.1093/NAR/20.22.6115.

Murat, C., Payen, T., Noel, B., Kuo, A., Morin, E., Chen, J., Kohler, A., Krizsán, K., Balestrini, R., Da Silva, C., Montanini, B., Hainaut, M., Levati, E., Barry, K.W., Belfiori, B., Cichocki, N., Clum, A., Dockter, R.B., Fauchery, L., Guy, J., Iotti, M., Le Tacon, F., Lindquist, E.A., Lipzen, A., Malagnac, F., Mello, A., Molinier, V., Miyauchi, S., Poulain, J., Riccioni, C., Rubini, A., Sitrit, Y., Splivallo, R., Traeger, S., Wang, M., Žifčáková, L., Wipf, D., Zambonelli, A., Paolocci, F., Nowrousian, M., Ottonello, S., Baldrian, P., Spatafora, J.W., Henrissat, B., Nagy, L.G., Aury, J.M., Wincker, P., Grigoriev, I.V., Bonfante, P., Martin, F.M., 2018. Pezizomycetes genomes reveal the molecular basis of ectomycorrhizal truffle lifestyle. Nat. Ecol. Evol. 2, 1956–1965. https://doi.org/10.1038/s41559-018-0710-4.

Nordbring-Hertz, B., Stålhammar-Carlemalm, M., 1978. Capture of nematodes by *Arthrobotrys oligospora*, an electron microscope study. Can. J. Bot. 56, 1297–1307. https://doi.org/10.1139/B78-146.

Pace, H.C., Brenner, C., 2001. The nitrilase superfamily: classification, structure and function. Genome Biol. 2, 1–9. https://doi.org/10.1186/GB-2001-2-1-REVIEWS0001.

Opulente, D.A., LaBella, A.L., Harrison, M.C., Wolters, J.F., Liu, C., Li, Yonglin, Kominek, J., Steenwyk, J.L., Stoneman, H.R., VanDenAvond, J., Miller, C.R., Langdon, Q.K., Silva, M., Gonçalves, C., Ubbelohde, E.J., Li, Yuanning, Buh, K. V., Jarzyna, M., Haase, M.A.B., Rosa, C.A., ČCadež, N., Libkind, D., DeVirgilio, J.H., Hulfachor, A.B., Kurtzman, C.P., Sampaio, J.P., Gonçalves, P., Zhou, X., Shen, X.X., Groenewald, M., Rokas, A., Hittinger, C.T., 2024. Genomic factors shape carbon and nitrogen metabolic niche breadth across Saccharomycotina yeasts. Science 384, eadj4503. https://doi.org/10.1126/SCIENCE.ADJ4503.

Patil, S.P., Dalal, K.S., Shirsath, L.P., Chaudhari, B.L., 2023. Microbial hyaluronidase: its production, purification and applications, in: Verma, P. (Ed.), Industrial Microbiology and Biotechnology: Emerging Concepts in Microbial Technology. Springer Nature, Singapore, pp. 473–497. https://doi.org/10.1007/978-981-99-2816-3_16.

Pramer, D., 1964. Nematode-trapping fungi. Science 144, 382–388. https://doi.org/10.1126/SCIENCE.144.3617.382.

R Core Team, 2023. R: A language and environment for statistical computing.

Radkov, A.D., Hsu, Y.P., Booher, G., Vannieuwenhze, M.S., 2018. Imaging bacterial cell wall biosynthesis. Annu. Rev. Biochem 87, 991–1014. https://doi.org/10.1146/ANNUREV-BIOCHEM-062917-012921.

Raffa, N., Keller, N.P., 2019. A call to arms: Mustering secondary metabolites for success and survival of an opportunistic pathogen. PLoS Pathog. 15, e1007606. https://doi.org/10.1371/JOURNAL.PPAT.1007606.

Rampino, M.R., Eshet-Alkalai, Y., Koutavas, A., Rodriguez, S., 2020. End-Permian stratigraphic timeline applied to the timing of marine and non-marine extinctions. Palaeoworld 29, 577–589. https://doi.org/10.1016/J.PALWOR.2019.10.002.

Rohlfs, M., Churchill, A.C.L., 2011. Fungal secondary metabolites as modulators of interactions with insects and other arthropods. Fungal Genet. Biol. 48, 23–34. https://doi.org/10.1016/J.FGB.2010.08.008.

Romano, C., Goudemand, N., Vennemann, T., Ware, D., Schneebeli-Hermann, E., Hochuli, P., Brühwiler, T., Brinkmann, W., Bucher, H., 2013. Climatic and biotic upheavals following the end-Permian mass extinction. Nature Geosci 6, 57–60. https://doi.org/10.1038/ngeo1667.

Sanderson, M.J., 2003. r8s: inferring absolute rates of molecular evolution and divergence times in the absence of a molecular clock. Bioinformatics 19, 301–302. https://doi.org/10.1093/bioinformatics/19.2.301.

Shen, S.Z., Crowley, J.L., Wang, Y., Bowring, S.A., Erwin, D.H., Sadler, P.M., Cao, C.Q., Rothman, D.H., Henderson, C.M., Ramezani, J., Zhang, H., Shen, Y., Wang, X.D., Wang, W., Mu, L., Li, W.Z., Tang, Y.G., Liu, X.L., Liu, L.J., Zeng, Y., Jiang, Y.F., Jin, Y.G., 2011. Calibrating the end-Permian mass extinction. Science 334, 1367–1372. https://doi.org/10.1126/science.1213454.

Shen, X.X., Steenwyk, J.L., LaBella, A.L., Opulente, D.A., Zhou, X., Kominek, J., Li, Y., Groenewald, M., Hittinger, C.T., Rokas, A., 2020. Genome-scale phylogeny and contrasting modes of genome evolution in the fungal phylum Ascomycota. Sci. Adv. 6, eabd0079. https://doi.org/10.1126/sciadv.abd0079.

Smith, S.D., Pennell, M.W., Dunn, C.W., Edwards, S.V., 2020. Phylogenetics is the new genetics (for most of biodiversity). Trends Ecol. Evol. 35, 415–425. https://doi.org/10.1016/J.TREE.2020.01.005.

Stamatakis, A., 2014. RAxML version 8: a tool for phylogenetic analysis and post-analysis of large phylogenies. Bioinformatics 30, 1312–1313. https://doi.org/10.1093/BIOINFORMATICS/BTU033.

Steenwyk, J., Rokas, A., 2017. Extensive copy number variation in fermentation-related genes among Saccharomyces cerevisiae wine strains. G3 7, 1475–1485. https://doi.org/10.1534/G3.117.040105/-/DC1.

Steenwyk, J.L., Buida, T.J., Li, Y., Shen, X.X., Rokas, A., 2020a. ClipKIT: a multiple sequence alignment trimming software for accurate phylogenomic inference. PLoS Biol. 18, e3001007. https://doi.org/10.1371/JOURNAL.PBIO.3001007.

Steenwyk, J.L., Li, Y., Zhou, X., Shen, X.X., Rokas, A., 2023. Incongruence in the phylogenomics era. Nat. Rev. Genet. 24, 834–850. https://doi.org/10.1038/S41576-023-00620-X.

Steenwyk, J.L., Lind, A.L., Ries, L.N.A., dos Reis, T.F., Silva, L.P., Almeida, F., Bastos, R.W., Fraga da Silva, T.F. de C., Bonato, V.L.D., Pessoni, A.M., Rodrigues, F., Raja, H.A., Knowles, S.L., Oberlies, N.H., Lagrou, K., Goldman, G.H., Rokas, A., 2020b. Pathogenic allodiploid hybrids of Aspergillus fungi. Curr. Biol. 30, 2507. https://doi.org/10.1016/j.cub.2020.04.071.

Steenwyk, J.L., Mead, M.E., Knowles, S.L., Raja, H.A., Roberts, C.D., Bader, O., Houbraken, J., Goldman, G.H., Oberlies, N.H., Rokas, A., 2020c. Variation among biosynthetic gene clusters, secondary metabolite profiles, and cards of virulence across Aspergillus Species. Genetics 216, 481–497. https://doi.org/10.1534/GENETICS.120.303549.

Sun, Y., Zulla, M.J., Joachimski, M., Bond, D.P., Wignall, P.B., Zhang, Z.T., Zhang, M.H., 2019. Ammonium ocean following the end-Permian mass extinction. Earth Planet. Sci. Lett. 518, 211–222. https://doi.org/10.1016/j.epsl.2019.04.036.

Tamura, K., Stecher, G., Kumar, S., 2021. MEGA11: molecular evolutionary genetics analysis version 11. Mol. Biol. Evol. 38, 3022–3027. https://doi.org/10.1093/molbev/msab120.

Tan, G., Muffato, M., Ledergerber, C., Herrero, J., Goldman, N., Gil, M., Dessimoz, C., 2015. Current methods for automated filtering of multiple sequence alignments frequently worsen single-gene phylogenetic inference. Syst. Biol. 64, 778–791. https://doi.org/10.1093/SYSBIO/SYV033.

Thumuluri, V., Almagro Armenteros, J.J., Johansen, A.R., Nielsen, H., Winther, O., 2022. DeepLoc 2.0: multi-label subcellular localization prediction using protein language models. Nucleic Acids Res. 50, 228–234. https://doi.org/10.1093/NAR/GKAC278.

Tunlid, A., Jansson, H.B., Nordbring-Hertz, B., 1992. Fungal attachment to nematodes. Mycol. Res. 96, 401–412. https://doi.org/10.1016/S0953-7562(09)81082-4.

van den Hoogen, J., Geisen, S., Routh, D., Ferris, H., Traunspurger, W., Wardle, D.A., de Goede, R.G.M., Adams, B.J., Ahmad, W., Andriuzzi, W.S., Bardgett, R.D., Bonkowski, M., Campos-Herrera, R., Cares, J.E., Caruso, T., de Brito Caixeta, L., Chen, X., Costa, S.R., Creamer, R., Mauro da Cunha Castro, J., Dam, M., Djigal, D., Escuer, M., Griffiths, B.S., Gutiérrez, C., Hohberg, K., Kalinkina, D., Kardol, P., Kergunteuil, A., Korthals, G., Krashevska, V., Kudrin, A.A., Li, Q., Liang, W., Magilton, M., Marais, M., Martín, J.A.R., Matveeva, E., Mayad, E.H., Mulder, C., Mullin, P., Neilson, R., Nguyen, T.A.D., Nielsen, U.N., Okada, H., Rius, J.E.P., Pan, K., Peneva, V., Pellissier, L., Carlos Pereira da Silva, J., Pitteloud, C., Powers, T.O., Powers, K., Quist, C.W., Rasmann, S., Moreno, S.S., Scheu, S., Setälä, H., Sushchuk, A., Tiunov, A. V., Trap, J., van der Putten, W., Vestergård, M., Villenave, C., Waeyenberge, L., Wall, D.H., Wilschut, R., Wright, D.G., Yang, J. in, Crowther, T.W., 2019. Soil nematode abundance and functional group composition at a global scale. Nature 572, 194–198. https://doi.org/10.1038/s41586-019-1418-6.

Vidal-Diez de Ulzurrun, G., Hsueh, Y.P., 2018. Predator-prey interactions of nematode-trapping fungi and nematodes: both sides of the coin. Appl. Microbiol. Biotechnol. 102, 3939–3949. https://doi.org/10.1007/S00253-018-8897-5/METRICS.

Visscher, H., Brinkhuis, H., Dilcher, D.L., Elsik, W.C., Eshet, Y., Looy, C.V., Rampino, M.R., Traverse, A., 1996. The terminal Paleozoic fungal event: evidence of terrestrial ecosystem destabilization and collapse. PNAS 93, 2155–2158. https://doi.org/10.1073/PNAS.93.5.2155.

Wang, R., Wang, J., Yang, X., 2015. The extracellular bioactive substances of Arthrobotrys oligospora during the nematode-trapping process. Biol. Control 86, 60–65. https://doi.org/10.1016/J.BIOCONTROL.2015.04.003.

Wickham, H., 2017. ggplot2 - Elegant Graphics for Data Analysis (2nd Edition). J Stat Softw 77, 1–3. https://doi.org/10.18637/jss.v077.b02.

Wu, Q., Zhang, H., Ramezani, J., Zhang, F.F., Erwin, D.H., Feng, Z., Shao, L.Y., Cai, Y.F., Zhang, S.H., Xu, Y.G., Shen, S.Z., 2024. The terrestrial end-Permian mass extinction in the paleotropics postdates the marine extinction. Sci. Adv 10, eadi7284. https://doi.org/10.1126/sciadv.adi7284.

Yang, C.T., de Ulzurrun, G.V.D., Pedro Gonçalves, A., Lin, H.C., Chang, C.W., Huang, T.Y., Chen, S.A., Lai, C.K., Tsai, I.J., Schroeder, F.C., Stajich, J.E., Hsueh, Y.P., 2020. Natural diversity in the predatory behavior facilitates the establishment of a robust model strain for nematode-trapping fungi. PNAS 117, 6762–6770. https://doi.org/10.1073/PNAS.1919726117.

Yang, E., Xu, L., Yang, Y., Zhang, X., Xiang, M., Wang, C., An, Z., Liu, X., 2012. Origin and evolution of carnivorism in the Ascomycota (fungi). PNAS 109, 10960–10965. https://doi.org/10.1073/PNAS.1120915109.

Yang, J., Wang, L., Ji, X., Feng, Y., Li, X., Zou, C., Xu, J., Ren, Y., Mi, Q., Wu, J., Liu, S., Liu, Y., Huang, X., Wang, H., Niu, X., Li, J., Liang, L., Luo, Y., Ji, K., Zhou, W., Yu, Z., Li, G., Liu, Y., Li, L., Qiao, M., Feng, L., Zhang, K.Q., 2011. Genomic and proteomic analyses of the fungus Arthrobotrys oligospora provide insights into nematode-trap formation. PLoS Pathog. 7, e1002179. https://doi.org/10.1371/journal.ppat.1002179.

Yang, L., Li, X., Bai, N., Yang, X., Zhang, K.Q., Yang, J., 2022. Transcriptomic analysis reveals that Rho GTPases regulate trap development and lifestyle transition of the nematode-trapping fungus Arthrobotrys oligospora. Microbiol Spectr 10. https://doi.org/10.1128/SPECTRUM.01759-21.

Yang, X., Ma, N., Yang, L., Zheng, Y., Zhen, Z., Li, Q., Xie, M., Li, J., Zhang, K.Q., Yang, J., 2018. Two Rab GTPases play different roles in conidiation, trap formation, stress resistance, and virulence in the nematode-trapping fungus Arthrobotrys oligospora. Appl. Microbiol. Biotechnol. 102, 4601–4613. https://doi.org/10.1007/S00253-018-8929-1.

Yang, Y., Yang, E., An, Z., Liu, X., 2007. Evolution of nematode-trapping cells of predatory fungi of the Orbiliaceae based on evidence from rRNA-encoding DNA and multiprotein sequences. PNAS 104, 8379–8384. https://doi.org/10.1073/PNAS.0702770104.

Zhang, H., Yohe, T., Huang, L., Entwistle, S., Wu, P., Yang, Z., Busk, P.K., Xu, Y., Yin, Y., 2018. dbCAN2: a meta server for automated carbohydrate-active enzyme annotation. Nucleic Acids Res. 46, W95–W101. https://doi.org/10.1093/NAR/GKY418.

Zhang, W., Chen, J., Fan, Y., Hussain, M., Liu, X., Xiang, M., 2021. The E3-ligase AoUBR1 in N-end rule pathway is involved in the vegetative growth, secretome, and trap formation in Arthrobotrys oligospora. Fungal Biol. 125, 532–540. https://doi.org/10.1016/J.FUNBIO.2021.02.003.

Zhang, W., Liu, D., Yu, Z., Hou, B., Fan, Y., Li, Z., Shang, S., Qiao, Y., Fu, J., Niu, J., Li, B., Duan, K., Yang, X., Wang, R., 2020. Comparative genome and transcriptome analysis of the nematode-trapping fungus Duddingtonia flagrans reveals high pathogenicity during nematode infection. Biol. Control 143, 104159. https://doi.org/10.1016/J.BIOCONTROL.2019.104159.

Zhu, Q., Kosoy, M., Dittmar, K., 2014. HGTector: an automated method facilitating genome-wide discovery of putative horizontal gene transfers. BMC Genomics 15. https://doi.org/10.1186/1471-2164-15-717.